Processing of Open Porous Zirconia via Alkane-Phase Emulsified Suspensions for Plasma Applications

Emad M. M. Ewais*

Refractory and Ceramic Materials Division (RCMD), Central Metallurgical Research and Development Institute (CMRDI), Helwan, 11421 Cairo, Egypt

Suelen Barg and Georg Grathwohl

Ceramic Materials and Components, University of Bremen, D-28359 Bremen, Germany

Abdo A. Garamoon

Center of Plasma Technology, Al-Azhar University, Nasr City, Cairo, Egypt

Nasser N. Morgan

Physics Department, Faculty of Science (male), Al-Azhar University, Nasr City, Cairo, Egypt

Processing of porous zirconia by direct foaming of emulsified ceramic powder suspensions was examined. Surfactant stabilized heptane droplets were homogeneously dispersed in the aqueous suspension with maximum solids loading of zirconia powder. The porosity of the sintered porous parts increased with the amount of heptane in the emulsified suspensions. On the other hand, the bending strength increased with the decreasing heptane content. Porous zirconia samples were used as a dielectric barrier in an atmospheric pressure plasma system. The plasma system was powered by different applied voltages at 50 Hz using air as a working gas. Filamentary discharge mode was observed in all samples at a limit value of the applied voltage (breakdown voltage). Samples with high concentration of pores and suitable pore size exhibited a glow discharge mode beside the filamentary discharge mode. The effect of the porosity of zirconia on the formation of the glow discharge mode was discussed.

Introduction

Porosity is often considered as a problematic feature of technical ceramics. It offers, on the other hand, a high potential for innovative functions and a rising multitude

*dr_ewais@hotmail.com

of applications for high-performance ceramics, which are functionalized by adjusted porosity parameters. In particular, the opportunities to merge several advantages inherent to the crystal structure with morphological features realized in the microstructure are seized by materials scientists at present to develop new porous ceramic components. Unique properties in terms of low density, low thermal conductivity, high gas permeability, large surface area, strong thermal shock resistance, refractoriness, and high mechanical stiffness offered by porous ceramics are of technological interest. These properties have the potential to be used in a wide range of applications such as filtration, catalysis, thermal insulation, biomedical implants, gas burners, fuel-cell electrodes, preform for metal–ceramic composites, impact-absorbing structures, absorbents, photonic crystals, and gas sensors.[1–28]

The capability of such porous components to perform successfully under the intended application conditions depends often directly on the porosity, pore size distribution, pore morphology, and orientation. There is then a strong need to control these porosity parameters in order to achieve superior properties of the components.[29,30] Several technologies were developed to manufacture strong and reliable porous ceramics. Among the various processing techniques for fabrication of porous ceramics, the four most common methods can be divided into two groups. The first two approaches lead mainly to pore sizes in the range of 2–100 nm; they use the incorporation of organic phases, which are then eliminated during firing[31] and the partial sintering of ceramics.[32] These processes produce ceramics with combinations of micro-, meso-, and macroporosity. The other two approaches typically produce cellular structures with pores varying from approximately 10 μm to several millimeters; they apply the replication of polymer foams by impregnation[33] or CVD coating[34] and direct foaming of suspensions.[35–37] Porous ceramic materials produced by the replication method have poor mechanical properties due to highly open pore structures and hollow struts left behind from the burning of polyurethane. Although there are a number of routes for the processing of porous ceramics, as mentioned above, direct foaming of emulsified inorganic powder suspensions has been shown as an efficient way to produce cellular ceramics presenting excellent mechanical properties due to the defect free build-up of the struts and particularly tailored microstructural features as highly interconnected cells.[38–41]

In this innovative process, an alkane phase is homogeneously emulsified in a stabilized aqueous ceramic powder suspension giving rise to low-alkane-phase emulsified suspensions[38] or high-alkane-phase emulsified suspensions (HAPES)[39] depending on the dispersed phase content. In contrast to the more conventional direct foaming methods, foaming here is provided by the evaporation of the emulsified alkane droplets. The emulsified suspensions can be simply consolidated by the expansion of the alkane droplets due to foaming and concurrent drying. Alternatively, freeze casting/gelation techniques can be applied as further means of consolidation (Soltmann et al., unpublished data). If the physical conditions are favorably adjusted, this new process leads to a time-dependent expansion of the emerging foam resulting in the controlled formation of macro- and microstructures with interconnected cells ranging from a low micrometer scale to 3000 μm.

The versatility of the method is reflected by the possibility of processing various inorganic powder surface chemistries into designed cellular structures including gradients, required for specific technological applications.[40–42]

Zirconia presents high mechanical strength and fracture toughness, excellent wear resistance as well as a strong resistance against corrosion and chemicals. Further more, it has good biocompatibility and provides high efficiencies as a solid electrolyte for gas sensor and other active functions in fuel cells and batteries. Consequently, the development of highly porous zirconia is very desirable for several technological applications including environments at high temperatures. Particular attention is given to the porous burners' field where severe thermal loadings including thermal gradients and transients have to be envisaged.[43] In spite of this, only few works on the processing of porous zirconia have been published so far[43–45] and nondealing with direct foaming techniques.

Recently, porous materials have been used in the field of plasma physics as dielectric materials to realize glow discharge at atmospheric pressure.[46] Plasma sources operating at atmospheric pressure have attracted much attention in the field of application of plasma technology in industry, environment, and medicine because of their economical benefits of getting rid of high-cost vacuum systems and low running costs. Therefore, extensive studies are now devoted to atmospheric pressure glow discharges (APGDs) using mostly dielectric barrier discharge (DBD) schemes.[47–50]

Atmospheric pressure discharges controlled by solid dielectrics known as DBD have been used for a long time for various industrial applications: ozone generator, excimer lamp, plasma display panel, and surface treatment. The main problems of the usage of DBD in different applications are the homogeneity and the stability of the discharge. Recently, homogeneous and stable discharges at atmospheric pressure, called glow dielectric barrier discharge or APGD have been obtained in helium, argon, or nitrogen.[51,52] The transition from one discharge to the other one does not only depend on the type of gas and the dielectric material but also on the slope of the excitation and the power supply characteristics including their intrinsic imperfections.[51] Obtaining uniform and stable discharges in open air is one of the most remarkable achievements in the plasma field research. Generally, to generate glow discharge in air, sufficient numbers of seed electrons are needed. But in the presence of electronegative gases, such as oxygen and water vapor, atmospheric discharges exist as streamer and nonuniform microdischarges (filamentary discharge). Therefore, most of APGDs are generated in other gases, such as He, Ar, and N_2.[52] In these discharges, metastable species of each gas prevent an electron avalanche that induces streamer discharge. These neutral metastable species with long lifetimes move around unrelated to the applied electric field and transfer their energies by collision with other atoms or molecules. Afterwards, every region of the plasma zone becomes uniform and stable.[53] However, in the case of air discharge, oxygen molecules (representing 21% of air constituents) quench nitrogen metastable species, and hence atmospheric discharges exist as filamentary discharges. Successful efforts to minimize this quenching effect, by modifying the reactor geometry,[54–59] or applying fast gas flow were reported.[53] The formation of APGD in air at 50 Hz has been obtained recently using an alumina ceramic of a special configuration as a dielectric.[46]

Therefore, in this paper, open porous zirconia presenting remarkable bending strength and controlled porosity parameters is developed by the direct foaming process based on the transition of emulsified suspensions into cellular ceramics. For the first time, the capability of porous zirconia ceramics and the effects of pore concentration and dimensions on the realization APGD in open air at 50 Hz are explored.

Materials and Experimental Procedure

Materials

Zirconia powder (Zirconia-TZ-3Y) used in this work was obtained from Tosoh Corporation (Tosoh, Tokyo, Japan). The powder contains 5 wt% yttria for stabilization of the tetragonal phase. Chemical analysis of the supplied powder (provided by supplier) revealed the following composition (mass%): minimum 94.117 ZrO_2, 5.17 Y_2O_3, maximum 0.005 Al_2O_3, 0.002 Fe_2O_3, 0.005 SiO_2, 0.021 Na_2O, and 0.68 ignition loss. The powder has a BET surface area of 15.4 m^2/g and allows a sintering density of 6.05 g/cm^3. The initial particle size distribution is characterized by $d_{10} = 5\,\mu m$, $d_{50} = 0.7\,\mu m$, and $d_{90} = 0.2\,\mu m$ (as measured with using an L.S. particle size analyzer). Tri-ammonium citrate (TAC, Aldrich, St. Louis, MO) was used as a dispersing agent (supplied by Aldrich). Sodium lauryl sulfate, commercially available as Lutensit 2230 (BASF) has been used as an anionic surfactant.

Porous Zirconia Preparation Process

An aqueous suspension containing 40 vol% powder with 0.4 mass% (on powder basis) TAC (Aldrich) was prepared. This quantity of the dispersant was proved to be sufficient to reach a well-dispersed medium and high solids loading (40 vol%) based on our previous work.[60] The suspension was prepared by mixing deionized water, TAC, and zirconia powder in a laboratory mixer (Dispermat LC, VMA Getzmann, Reichshof, Germany) with a 30 mm dispersing tool operating at a mixing velocity of 2800 rpm for 20 min. The pH of the suspension after preparation was measured as 8.7. Afterwards the suspensions were subjected to deaeration to remove undesired entrapped bubbles. This procedure was performed in a container under reduced pressure (5 kPa).

In this work, 30, 50, and 70 vol% heptane and 1.6 vol% surfactant (based on heptane content) were subsequently added to deaired zirconia suspensions (40 vol% solids). Mixing was then achieved by mechanical stirring for 2.5 min at 2500 rpm under reduced pressure (10 kPa) to avoid air bubble incorporation during emulsification. This pressure was chosen taking into account the vapor pressure of heptane (4.6 kPa at 20°C) to avoid its evaporation during this stage.

The composition was chosen so that even by moderated heptane concentrations (30 vol%), minimal

bubble growth occurs during foaming, which is typical for HAPES.[39]

The emulsified suspensions were poured in plastic round molds with diameters of 50 and 80 mm, respectively, and a height of 15 mm and then left at ambient temperature (20°C) for 24 h. After the consolidation, the zirconia foams were preheated to 400°C with 0.5 K/min and then sintered at 1450°C for 1 h. The heating (400–1450°C) and cooling rates were 5 K/min.

Structural and Mechanical Characterization

Microstructural characterization of open porous zirconia samples was performed using scanning electron microscope (Model CAM SCAN, Cambridge Scanning, Cambridge, U.K.). Cell sizes were measured from planar sections with the linear intercept method using the software Lince (TU Darmstadt, Darmstadt, Germany). The average cell size d_{50}, as well as d_{10} and d_{90} were determined from the cumulative cell size distribution curves, corresponding to the cell diameter at a cumulative percentage of 50%, 10%, and 90% (number distribution). The window size distribution was measured using Hg-Intrusion (Pascal 140/440, CE Instruments, Hofheim, Germany). The volumetric density ρ_v of the foams was determined from the mass and dimensions of the sintered bodies. The volumetric porosity P was calculated from $P = 1-\rho_v/\rho_t$, where ρ_t is the theoretical density of zirconia (6.05 g/cm^3). Three-point bending strength has been performed using zwick/roell instrument with a span of 30 mm and at a constant crosshead speed of 1 mm/min. The tests were performed at room temperature. The size samples were 40 mm $\times$ 5 mm $\times$ 4.7 mm. The time of all sample failure was 8–10 s. The three-point bending strength (S) was calculated from $S = 3PL/2bd^2$, where P is the maximum force, L is span length, b is sample width, and d is the sample thickness. An average value was obtained from the four samples tested for each case.

Experimental Setup of APGD System

The discharge cell as shown in Fig. 1 consists of two copper plane-parallel electrodes of 3 cm diameter. One of the two electrodes was covered by a ceramic plate of porous zirconia with a diameter of 1 cm, a thickness of 0.5 cm, pores concentration of 35%, 54%, and 70%, and an average window diameter of 0.6, 1.4, and 1.2 μm, respectively. The distance between the two dielectric plates was 0.5 mm. The discharge was operated in open air under atmospheric pressure.

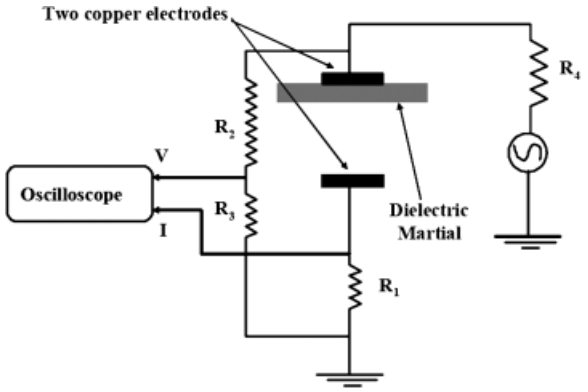

Fig. 1. Schematic diagram of the discharge cell.

The discharge cell was connected to an ac transformer (1–10 kV) that generates sinusoidal voltage with a frequency of 50 Hz. The applied potential (V_a) across the electrodes, and the current (I) passing through the system were recorded using a digital oscilloscope (HAMEG HM407—40 MHz). The current was measured by the voltage drop across the resistance R_1 ($= 100\,\Omega$) connected in series with the discharge system to the ground as shown in Fig. 1. The voltage across the two electrodes was also measured using the potential divider of the resistance system R_2, R_3 where $R_2/R_3 = 500$. The equivalent electric circuit in dielectric-controlled APGD is shown in Fig. 2.

A voltage-controlled current source (G_g) provides an increasing current as long as the applied voltage across the cell gap exceeds the gas breakdown value, V_b. The current characteristic is a function of the applied voltage υ_T (t).

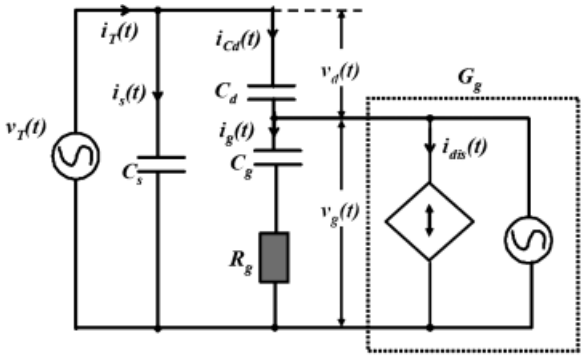

Fig. 2. Equivalent electric circuit of the dielectric barrier discharge discharge.

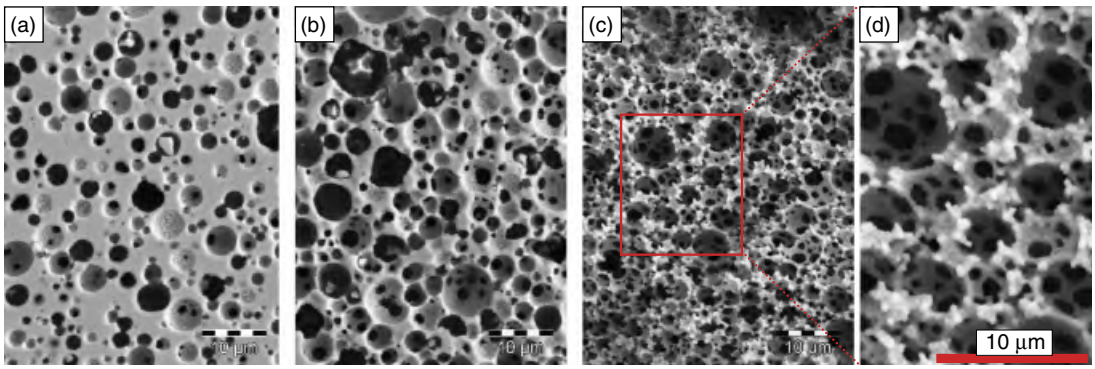

Fig. 3. Microstructure of sintered zirconia foams produced from emulsified suspensions containing 30 vol% (a), 50 vol% (b), and 70 vol% (c, d) heptane as dispersed phase.

$$v_T(t) = v_d(t) + v_g(t)$$

$$i_T(t) = i_s(t) + i_{C_d}(t)$$

$$i_{C_d}(t) = i_{dis}(t) + i_g(t)$$

$$i_s(t) = C_s \frac{dv_T(t)}{dt},\ i_d(t) = C_d \frac{dv_T(t)}{dt}$$

$$i_T(t) = C_s \frac{dv_T(t)}{dt} + C_d \frac{dv_T(t)}{dt}$$

where $v_T(t)$ is the total applied voltage, C_d is the dielectric capacitance, C_g is the gas capacitance, $i_g(t)$ is the displacement current across the gas, C_s is the stray capacitance of the cell, and $i_{dis}(t)$ is the discharge current.

Results and Discussion

Processing of Porous Zirconia with Controlled Microstructures

In HAPES, the control of droplet size and concentration is decisive for the control of the microstructural parameters.[39,41] The transition of the stable emulsified suspensions to stable green bodies is achieved by the evaporation of the alkane phase due to minimum foam growth.

The microstructures of the sintered zirconia foams produced from emulsified suspensions composed of 30, 50, and 70 vol% heptane are shown in Fig. 3. The quantitative analysis of microstructural parameters and bending strength is summarized in Table I. The heptane content controls the droplet concentration in emulsified suspensions and the cell concentration in the sintered foams. Consequently, the porosity could be adjusted between 35% and 70% by the adjustment of heptane content between 30 and 70 vol%.

The connection between adjacent cells (windows) is provided by the thin films between the evaporating heptane droplets in the wet stage. The window number and size constitute the interconnectivity between cells. With the increase of cell density (number of cells per volume) and decreasing film thickness, the number of windows in the cell walls increases due to the higher specific surface area to be covered by the solid particles. Highly interconnected cells are then formed by 70 vol% heptane (Fig. 3c and d).

Table I. Zirconia Foams Microstructural Parameters and Bending Strength as a Function of Heptane Content in Emulsified Suspensions

Decane content (vol%)	Porosity (%)	Cell size d_{10}, d_{50}, d_{90} (µm)	Window size d_{50} (µm)	Bending strength (MPa)
30	35	1.2, 2.4, 4.0	0.6	105
50	54	1.9, 3.5, 5.8	1.4	93
70	70	1.8, 2.5, 4.0	1.2	77

In spite of the variation in heptane content, the average cell size d_{50} was maintained between 2.4 and 3.5 μm. Actually, the ratio between interfacial and shear stresses during droplet break up will determine the droplet and consequently the cell size in HAPES.[39] Here, the constant stirring rate during emulsification appears to act as a main influence on the droplet size.

In a previous work, the window size in highly concentrated emulsified suspensions (70 vol% alkane) was reported to be proportional to the cell size.[41] In our studies, we have seen that the window size also depends on the ratio between particles and the droplet surface area to be covered by them. Emulsified suspensions containing 30 vol% alkane resulted in a smaller average window size d_{50} (0.6 μm) than in the case of 50 and 70 vol% alkane (1.4–1.2 μm). This could be attributed to the reduced contact between adjacent droplets because of the lower droplet packing as well as the lower specific surface area, enabling a higher cover of particles on the droplet surface. In the case of 50 and 70 vol% alkane, the window size is proportional to the cell size.

The materials present a remarkable bending strength between 77 and 105 MPa and a moderate influence of the porosity on strength (Table I).

Voltage and Current WaveForms

Voltage and current waveforms of the DBD were recorded on the oscilloscope for three samples of zirconia (refer to Table I) as a dielectric material with air as a working gas under atmospheric pressure. The results are demonstrated in Figs 4–6 as voltage and current oscillograms for air discharge under atmospheric pressure and at applied voltages with a gap space of 0.5 mm. The DBD performance under application of zirconia plates with the lowest porosity (35%) and window size (0.6 μm) as dielectric electrode is illustrated in Fig. 4 for applied voltages of 2.5 kV (a), 3 kV (b), and 3.5 kV (c). From the figures, it can be seen that a streamer discharge was formed, which is characterized by discrete current spikes. These spikes were related to the formation of microdischarges (filaments) of tens of nanosecond duration in the gap space.[61] They start when the breakdown field is reached locally and extinguish (turn off) when the field is reduced to such an extent that electron attachment and recombination dominate over ionization. These microdischarges are randomly distributed in the discharge area. The peak of each individual spike is related to the number of instantaneous microfilaments

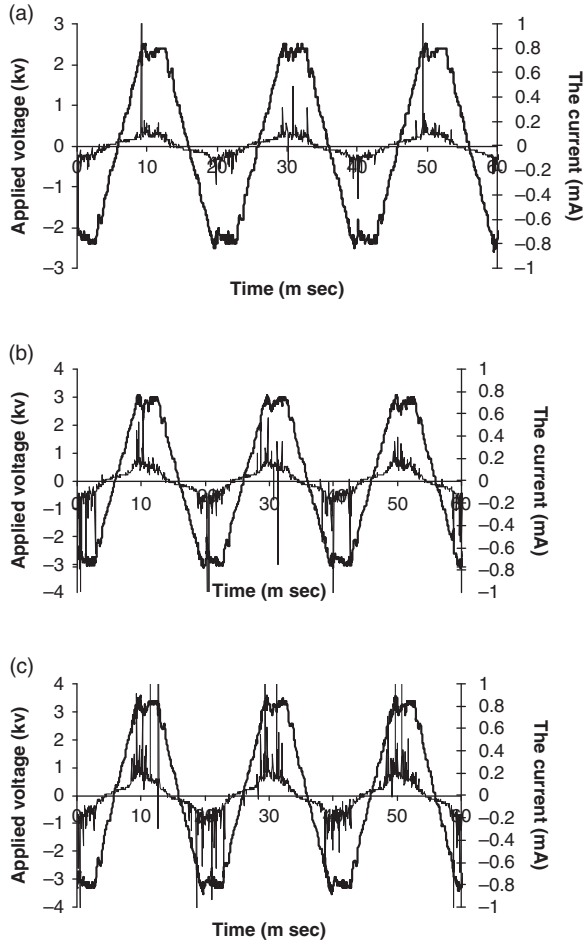

Fig. 4. Current voltage waveform for sample 1 (window size 0.6 μm, porosity 35%) at different applied voltages.

that were formed at this instant, and hence a high current spike indicates that a high number of microdischarges are initiated almost simultaneously. It can be noticed that, when the external voltage rises, additional microdischarges are formed at new positions because the presence of residual charges on the dielectric has reduced the electric fields at positions where the microdischarges have already occurred. Because high voltages at low frequency tend to spread the microdischarges and increase the number of instantaneous filaments,[62] the peaks of the spikes increase by increasing the peak of the applied voltage. Sample 1 shows no abnormal behavior compared with any other dielectric material used in DBD.

Increasing the porosity, the cell, and window size in sample 2 leads to filamentary discharge superimposed on

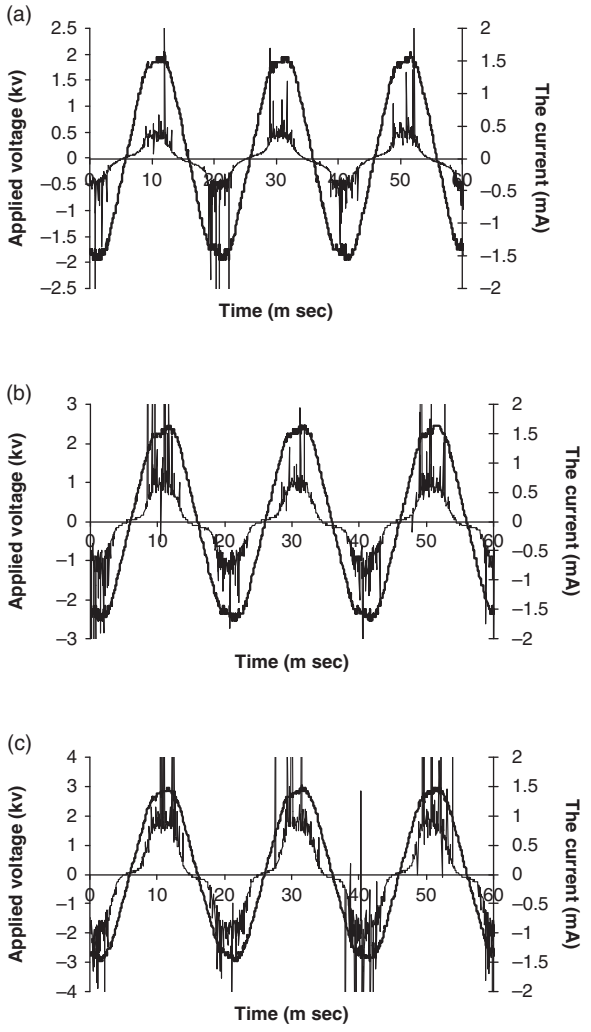

Fig. 5. Current voltage waveform for sample 2 (window size 1.4 μm, porosity 54%) at different applied voltages.

glow discharge as shown in Fig. 5b and c. This discharge is characterized by a diffuse APGD discharge, which spreads in the discharge gap between the two electrodes. One requirement for establishing a volume-stabilized glow discharge is that the preionization electron density is large enough to cause an appreciable overlap and coalescence of primary avalanche heads and smoothing of space-charge field gradients at the stage when streamer formation would otherwise occur. The glow discharge formed in sample 2 may be attributed to the existence of a high concentration of pores (54%) filled with air that undergo a discharge when the applied voltage reaches a limit value (breakdown voltage). The dimension of the window (1.4 μm) and *pd* value inside the window equals about 0.1 torr cm, which is corresponding to a breakdown voltage of about 1.5 kV. In sample 1, the pd value inside the window equals about 0.04 torr cm, which is corresponding to a breakdown voltage much higher than 2 kV,[63] where *p* is the gas pressure inside the pores and *d* is the length of the discharge channel (in our case, it is the diameter of the pore).

Figure 6a–c shows the current and voltage waveforms for sample 3 (porosity 70% and window size 1.2 μm). It can be observed that sample 3 exhibits the same behavior as sample 2 where the glow discharge mode appears beside the filamentary discharge mode.

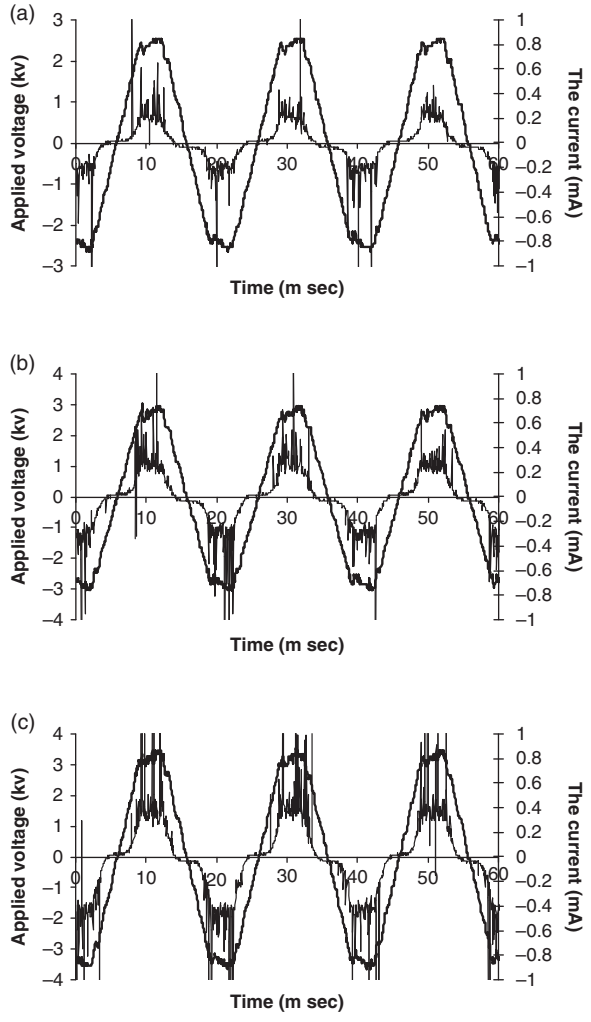

Fig. 6. Current voltage waveform for sample 3 (window size 1.2 μm, porosity 70%) at different applied voltages.

The formation of glow discharge mode in samples 2 and 3 can be referred to the high concentration of the pores (54% and 70%) and relatively low breakdown voltage inside the windows (1.5, 1.6 kV). Because the windows contain air, a discharge occurs in the microwindows and a current will flow inside these windows when the voltage drop across a window reaches the gas breakdown voltage. This current is very important in sustaining the glow discharge mode through two ways[46]:

(a) During the discharge inside the microwindows, the electron current flows and approaches the zirconia surface, which increases the probability of the electron emission from the zirconia surface and in turn increases the primary seed electrons. Seed electrons initiate the growing up of the glow discharge mode.

(b) Discharging the gas inside the windows means decreasing the voltage drop across the windows and hence the voltage drop across the dielectric material, which in turn increases the voltage applied to the gas in the gap space.

Conclusions

Open porous zirconia foams with average cell sizes between 2.4 and 3.5 μm and window sizes between 0.6 and 1.4 μm have been produced by a versatile and simple route based on the direct foaming of stable emulsified powder suspensions. The porosity could be controlled by the heptane content, between 35% and 70%. The materials yielded to a remarkable bending strength between 77 and 105 MPa.

Furthermore, the developed materials have been used as dielectric barriers to generate atmospheric pressure plasma. The formation of APGD plasma has been realized in open air at 50 Hz using porous zirconia with high porosity between 54% and 70%. *I–V* waveforms of the discharge have confirmed the presence of APGD. At low porosity (35%), the APGD has not been formed and the discharge appeared almost as a filamentary discharge. The window size has been found to play an important role in the formation of APGD via minimizing the breakdown voltage inside the pores. It has been found that the discharges inside the porous zirconia and on its surface provide sufficient seed electrons for obtaining a uniform and stable glow discharge mode.

References

1. F. F. Lange and K. T. Miller, "Open Cell, Low-Density Ceramics Fabricated from Reticulated Polymer Substrates," *Adv. Ceram. Mater.*, 2 827–831 (1987).
2. J. Saggio-Woyansky, C. E. Scott, and W. P. Minnear, "Processing of Porous Ceramics," *Am. Ceram. Soc. Bull.*, 71 [11] 1674–1682 (1992).
3. D. Trimis and F. Durst, "Combustion in a Porous Medium—Advances and Applications," *Combust. Sci. Technol.*, 121 153–168 (1996).
4. P. Sepulveda, "Gelcasting of Foams for Porous Ceramics," *Am. Ceram. Soc. Bull.*, 76 [10] 61–65 (1997).
5. P. Colombo and J. R. Hellmann, "Ceramic Foams from Preceramic Polymers," *Mater. Res. Innovat.*, 6 260–272 (2002).
6. M. Scheffler, and P. Colombo, eds., *Cellular Ceramics: Structure, Manufacturing, Properties and Applications*, Wiley-VCH, Weinheim, 2005.
7. A. R. Studart, U. T. Gonzenbach, E. Tervoort, and L. J. Gauckler, "Processing Routes to Macroporous Ceramics—A Review," *J. Am. Ceram. Soc.*, 89 [6] 1771–1789 (2006).
8. P. Colombo, "Conventional and Novel Processing Methods for Cellular Ceramics," *Philos. Trans. Roy. Soc. A*, 364 [1838] 109–124 (2006).
9. L. Biasetto, P. Colombo, M. D. M. Innocentini, and S. Mullens, "Gas Permeability of Microcellular Ceramic Foams," *Ind. Eng. Chem. Res.*, 46 3366–3372 (2007).
10. K. Ishizaki, S. Komarneni, and M. Nauko, *Porous Materials Process Technology and Applications*, Kluwer, London, U.K., 1998.
11. Y. Zhang, S. Zha, and M. Liu, "Dual-Scale Porous Electrodes for Solid Oxide Fuel Cells from Polymer Foams," *Adv. Mater.*, 17 487–491 (2005).
12. F. Chen, C. Xia, and M. Liu, "Preparation of Ordered Macroporous $Sr_{0.5}Sm_{0.5}CoO_3$ as Cathode for Solid Oxide Fuel Cells," *Chem. Lett.*, 10 1032–1033 (2001).
13. J. C. Ruiz-Morales, J. Canales-Vazquez, J. Pena-Martinez, D. M. Lopez, and P. Nunez, "On the Simultaneous Use of $La_{0.75}Sr_{0.25}Cr_{0.5}Mn_{0.5}O_{3-\delta}$ as Both Anode and Cathode Material with Improved Microstructure in Solid Oxide Fuel Cells," *Electrochimica Acta*, 52 278–284 (2006).
14. J. C. Ruiz-Morales, J. Canales-Vazquez, J. Pena-Martinez, D. Marrero-Lopez, J. T. S. Irvine, and P. Nunez, "Microstructural Optimisation of Materials for SOFC Applications Using PMMA Microspheres," *J. Mater. Chem.*, 16 540–542 (2006).
15. M. Boaro, J. M. Vohs, and R. J. Gorte, "Synthesis of Highly Porous Yttria-Stabilized Zirconia by Tape-Casting Methods," *J. Am. Ceram. Soc.*, 86 [3] 395–400 (2003).
16. S. Madhavi, C. Ferraris, and T. J. White, "Synthesis and Crystallization of Macroporous Hydroxyapatite," *J. Solid State Chem.*, 178 2838–2845 (2005).
17. C. Wang, A. Geng, Y. Guo, S. Jiang, X. Qu, and L. Li, "A Novel Preparation of Three-Dimensionally Ordered Macroporous M/Ti (M = Zr or Ta) Mixed Oxide Nanoparticles with Enhanced Photocatalytic Activity," *J. Colloid Interface Sci.*, 301 236–247 (2006).
18. N. Y. Yurii, A. Vlasov, and D. J. Norris, "Synthesis of Photonic Crystals for Optical Wavelengths from Semiconductor Quantum Dots," *Adv. Mater.*, 11 165–169 (1999).
19. S. H. Im, Y. T. Lim, D. J. Suh, and O. O. Park, "Three-Dimensional Self-Assembly of Colloids at a Water-Air Interface: A Novel Technique for the Fabrication of Photonic Bandgap Crystals," *Adv. Mater.*, 14 1367–1369 (2002).
20. J. E. G. J. Wijnhoven and W. L. Vos, "Preparation of Photonic Crystals Made of Air Spheres in Titania," *Science*, 281 [5378] 802–804 (1998).
21. R. W. Rice, *Porosity of Ceramics*, Marcel Dekker, New York, 1998.
22. L. J. Gibson and M. F. Ashby, *Cellular Solids, Structure, and Properties, Cambridge Solid State Science Series*, 2nd edition, Cambridge University Press, Cambridge, U.K., 1997.
23. D. J. A. Netz, P. Sepulveda, V. C. Pandolfelli, A. C. C. Spadaro, J. B. Alencastre, M. V. L. B. Bentley, J. M. Marchetti, "Potential Use of Gelcasting Hydroxyapatite Porous Ceramic as an Implantable Drug Delivery System," *Int. J. Pharm.*, 213 [1–2] 117–125 (2001).
24. L. A. Strom, T. B. Sweeting, D. A. Norris, and J. R. Morris, "Novel Application of Fully Sintered Reticulated Ceramics," *Mater. Res. Symp. Proc.*, 371 321–326 (1995).
25. R. L. Coble and W. D. Kingery, "Effect of Porosity on Physical Properties of Alumina," *J. Am. Ceram. Soc.*, 39 [11] 377–385 (1956).

26. H. Sherman, R. H. Tuffias, and R. B. Kaplan, ''Refractory Ceramic Foams: A Novel, New High-Temperature Structure,'' *Am. Ceram. Soc. Bull.*, 70 [6] 1025–1029 (1991).
27. B. John, ''Manufacture, Characterization and Application of Cellular Metals and Metal Foams,'' *Prog. Mater. Sci.*, 46 559–632 (2001).
28. X. Zhu, D. Jiang, S. Tan, and Z. Zhang, ''Improvement in the Strut Thickness of Reticulated Porous Ceramics,'' *J. Am. Ceram. Soc.*, 84 [7] 1654–1656 (2001).
29. M. E. Davis, ''Ordered Porous Materials for Emerging Applications,'' *Nature*, 417 813–821 (2002).
30. Y. W. Kim, S. H. Kim, H. D. Kim, and C. B. Park, ''Processing of Closed-Cell Silicon Oxycarbide Foams from a Preceramic Polymer,'' *J. Mater. Sci.*, 39 5647–5652 (2004).
31. S. Kormarneni, L. Pach, and R. Pidugu, ''Porous α-Alumina Ceramics Using Boehmite and Rice Flour,'' *Mater. Res. Soc. Symp. Proc.*, 371 285–290 (1995).
32. M. D. Lehigh and I. Nettleship, ''Microstructural Evolution of Porous Ceramics,'' *Mater. Res. Soc. Symp. Proc.*, 371 315–320 (1995).
33. W. P. Minnear, ''Processing of Porous Ceramics,'' *Ceram. Trans.*, 26 146–156 (1992).
34. Y. S. Lin and A. J. Burggraaf, ''CVD of Solid Oxides in Porous Substrates for Ceramic Membrane Modification,'' *AIChem J.*, 38 [3] 445–454 (1992).
35. M. Wu, T. Fujiu, and G. L. Messing, ''Synthesis of Cellular Inorganic Materials by Foaming Sol–Gels,'' *J. Non-Cryst. Solid*, 121 407–412 (1990).
36. S. J. Powell and J. R. G. Evans, ''The Structure of Ceramic Foams Prepared from Polyurethane-Ceramic Suspensions,'' *Mater. Manufact. Processes*, 10 [4] 757–771 (1995).
37. BASF European Patent Application, ''Ceramic Foam,'' No. 0330963, 1989.
38. S. Barg, C. Soltmann, M. Andrade, D. Koch, and G. Grathwohl, ''Cellular Ceramics by Direct Foaming of Emulsified Ceramic Powder Suspensions,'' *J. Am. Ceram. Soc.*, 91 [9] 2823–2829 (2008).
39. S. Barg, E. G. de Moraes, D. Koch, and G. Grathwohl, ''New Cellular Ceramics from High Alkane Phase Emulsified Suspensions (HAPES),'' *J. Eur. Ceram. Soc.*, 29 [12] 2439–2446 (2009).
40. S. Barg, C. Soltmann, D. Koch, and G. Grathwohl, ''Novel Open Cell Aluminum Foams and their Use as Reactive Support for Zeolite Crystallization,'' *J. Porous Mater.*, (2010), doi: 10.1007/s10934-010-9359-312.
41. S. Barg, D. Koch, and G. Grathwohl, ''Processing and Properties of Graded Ceramic Filters,'' *J. Am. Ceram. Soc.*, 92 [12] 2854–2860 (2009).
42. J. Hüppmeier, S. Barg, M. Baune, G. Grathwohl, and J. Thöming, ''Oxygen Feed Membranes in Autothermal Steam-Reformers—a Robust Temperature Control,'' *Fuel*, 89 [6] 1257–1264 (2010).
43. S. Gómez, J. Escobar, O. Alvarez, C. Rambo, A. de Oliveira, and D. Hotza, ''ZrO_2 Foams for Porous Radiant Burners,'' *J. Mater. Sci.*, 44 [13] 3466–3471 (2009).
44. C. Hong, X. Zhang, J. Han, J. Du, and W. Han, ''Ultra-High-Porosity Zirconia Ceramics Fabricated by Novel Room-Temperature Freeze-Casting,'' *Scripta Materialia*, 60 [7] 563–566 (2009).
45. M. P. Albano, L. A. Genova, L. B. Garrido, and K. Plucknett, ''Processing of Porous Yttria-Stabilized Zirconia by Tape-Casting,'' *Ceram. Int.*, 34 1983–1988 (2008).
46. A. A. Garamoon and D. M. El-zeer, ''Atmospheric Pressure Glow Discharge Plasma in Air at Frequency 50 Hz,'' *Plasma Sources Sci. Technol.*, 18 [4] 045006.1–045006.8 (2009).
47. U. Kogelschatz, ''Dielectric-Barrier Discharges: Their History, Discharge Physics, and Industrial Applications,'' *Plasma Chem. Plasma Process.*, 23 [1] 1–46 (2003).
48. V. Schulz-von der Gathen, ''Atmospheric Pressure Glow Discharges for Surface Treatment: Selected Examples,'' *XXVIIth ICPIG*, Eindhoven, the Netherlands, July 2005.
49. S. J . Scott, C. C. Figgures, and D. G. Dixon, ''Dielectric Barrier Discharge Processing of Aerospace Materials,'' *Plasma Sources Sci. Technol.*, 13 461–465 (2004).
50. Z. Machala, M. Janda, K. Hensel, I. Jedlovsky, L. Lestinska, V. Foltin, V. Martisovits, and M. Morvova, ''Emission Spectroscopy of Atmospheric Pressure Plasmas for Bio-Medical and Environmental Applications,'' *J. Mol. Spectrosc.*, 243 194–201 (2007).
51. F. Massines, R. Messaoudi, and C. Mayoux, ''Comparison between Air Filamentary and Helium Glow Dielectric Barrier Discharges for the Polypropylene Surface Treatment,'' *Plasmas Polym.*, 3 [1] 43–59 (1998).
52. J. H. Choi, T. Lee, I. Han, B. Oh, M. Jeong, J. Myoung, H. K. Baik, K. M. Song, and Y. S. Lim, ''Improvement of Plasma Uniformity Using ZnO-Coated Dielectric Barrier Discharge in Open Air,'' *Appl. Phy. Lett.*, 89 [8] 081501–081504 (2006).
53. N. Gherardi and F. Massines, ''Mechanisms Controlling the Transition from Glow Silent Discharge to Streamer Discharge in Nitrogen,'' *IEEE Trans. Plasma Sci.*, 29 [3] 536–544 (2001).
54. J. Tepper, M. Lindmayer, and J. Salge, ''Pulsed Uniform Barrier Discharges at Atmospheric Pressure,'' *HAKONE VI International Symposium on High Pressure Low Temperature Plasma Chemistry*, August 31, –September 2, 1998.
55. J. Tepper, P. Li, and M. Lindmayer, ''Effects of Interface Between Dielectric Barrier and Electrode on Homogeneous Barrier Discharges at Atmospheric Pressure,'' *XIV International Conference on Gas Discharges and Their Application*, Liverpool, September 1–6, 2002.
56. J. Tepper and M. Lindmayer, ''Investigations on Two Different Kinds of Homogeneous Barrier Discharges at Atmospheric Pressure,'' *HAKONE VII International Symposium on High Pressure Low Temperature Plasma Chemistry*, September 10–13, 2000.
57. J. Tepper, M. Lindmayer, and B. Juttner, ''Optical and Electrical Measurements of Homogeneous Barrier Discharges at Atmospheric Pressure,'' *XIII International Conference on Gas Discharges and Their Application*, September 3–8, 2000.
58. X. Wang, H. Luo, Z. Liang, T. Mao, and R. Ma, ''Influence of Wire Mesh Electrodes on Dielectric Barrier Discharge,'' *Plasma Sources Sci. Technol.*, 15 845–848 (2006).
59. T. Mao, *et al.*, ''Study of Homogeneous DBD with Fine Wire Meshes and PET Films in Air at Atmospheric Pressure,'' *28th ICPIG*, July 15–20, 2007.
60. E. Ewais, A. Zaman, and W. Sigmund, ''Temperature Induced Forming of Zirconia from Aqueous Slurries: Mechanism and Rheology,'' *J. Eur. Ceram. Soc.*, 22 [16] 2805–2812 (2002).
61. N. Gherardi, G. Gouda, E. Gat, A. Ricard, and F. Massines, ''Transition from Glow Silent Discharge to Micro-Discharges in Nitrogen Gas,'' *Plasma Sources Sci. Technol.*, 9 340–346 (2000).
62. U. Kogelschatz, B. Eliasson, and W. Egli, ''1997 Dielectric Barrier Discharges—Principle and Applications,'' *J. Physique*, IV C4 47–C4 66 (1997).
63. A. Von Engel, *Electric Plasmas their Nature and Uses*, Taylor & Francis, London, 1983.